


# The VIVA OpenHBM Finite Element 50th Percentile Female Occupant Model: Whole Body Model Development and Kinematic Validation

# The VIVA OpenHBM Finite Element 50th Percentile Female Occupant Model: Whole Body Model Development and Kinematic Validation

Jonas Östh, Manuel Mendoza-Vazquez, Astrid Linder, Mats Y Svensson, Karin Brolin *

***Abstract*** Recently, significant progress has been made in the development of Finite Element Human Body Models, and they have been introduced in the development of automotive safety systems. The average female has not been covered by previous modelling projects, although it has been shown that females are exposed to a higher risk of injury than males in comparable automotive accidents. This study aims to describe the development of a 50th percentile female Open Source Human Body Model, to validate its kinematics, and compare the effect of having a detailed or simplified neck model in the Model.

The Human Body Model was developed from surface data of a 50th percentile female, using rigid bones, kinematic joints, and deformable soft tissue for the whole body model, together with an existing detailed neck model and a new simplified neck model. The kinematic response was compared with female and scaled male Post Mortem Human Subject data using objective rating in frontal, roll-over, and rear-impact simulations. The model correlation was found to be 0.91, 0.67, and 0.63 in the principal direction of each load case. Using a simplified neck model only marginally influenced the correlation in whole body simulations, while in isolated-head neck simulations the head kinematics were affected.

***Keywords*** female, finite element, human body model, kinematics, rear-impact

## I. INTRODUCTION

Finite Element (FE) Human Body Models (HBMs) have a history of use for over 40 years in impact biomechanics research [1]. A milestone for FE HBM use in product development was the introduction of average male whole body HBMs such as the THUMS [2] and HUMOS [3] some 15 years ago. Since then, FE HBMs have been adopted by automotive manufacturers [4, 5] and suppliers[6], and are today complementing the traditional tools for development of safety systems, namely the Anthropomorphic Test Devices (ATDs). Using the FE method for modelling the human body rather than a mechanical model allows for a more detailed representation of all anatomical structures and in combination with detailed material models provides the ability for tissue level injury prediction. For instance, FE HBMs normally have a detailed skeleton, internal organs, and soft tissues, while ATDs are made of metal and rubber parts. In addition, ATDs are normally designed for one impact direction [7], while HBMs can be omnidirectional. The second generation whole body HBMs, i.e. the GHBMC [8– 11] and THUMS v4 [12] model series, provide a high level of detail and are validated for a large number of load cases with varied severity and direction [8–12].

At present, HBMs are also being considered for implementation into virtual test protocols [13], in which physical testing would be complemented or replaced by HBM simulations. For instance, virtual testing with HBMs would be advantageous in future complex loading scenarios, which would be challenging to reproduce in physical testing and for which ATDs are unlikely to provide biofidelic responses. The success of virtual test protocols requires HBM standardisation and procedures for handling the intellectual property of FE models provided by automotive manufacturers [13], for example. The present study concerns the development of a whole body FE HBM that is developed under the GPL v3 Open Source license [14]. A benefit of the Open Source approach for development of a HBM is the availability to the research community for joint model development and also has some potential for use in future virtual test protocols.

Anthropometric design criteria are commonly established to cover the 5th–95th percentiles of the user population [15]. This is reflected in the available HBMs, which typically represent the 50th percentile male [8, 12], and only recently the 5th percentile female[10] and the 95th percentile male[11]. However, the 50th percentile female is missing from the family of available models. This is not due to the lack of purpose for such a model. In their seminal work in the early 1980s Schneider *et al.*[16], who defined anthropometric design specifications for ATDs, argued that having both 50th percentile male and female ATDs would be optimal; even so, the 50th percentile female was omitted due to limited funding.

The effect of excluding 50th percentile female human models for impact biomechanics research and

*K. Brolin (karin.brolin@chalmers.se, +46 31 772 15 36) and M.Y. Svensson are Professors at Chalmers University of Technology and J. Östh and M. Mendoza-Vazquez were researchers at Chalmers University of Technology in Sweden. A. Linder is Research Director at the Swedish National Road and Transport Research Institute and an Adjunct Professor at Chalmers University of Technology.

development can be demonstrated by the findings of Kullgren *et al*. [17] who showed that reactive head restraint whiplash protection systems work for male occupants, but appear to have absolutely no effect for females. If models representing the female part of the population were available in the development and rating of such systems, it seems likely that this discrepancy in real-life protection would not exist.

Whiplash Associated Disorder (WAD) is the common denomination for a range of symptoms associated with cervical spine soft tissue injury that commonly result from low severity vehicle collisions. The risk for females to sustain WAD symptoms is, on average, double that of males, and even higher in similar crash conditions [18–24]. As the injured female population is close to the 50$^{th}$ percentile female [18] in stature and weight, the 5$^{th}$ percentile female human models available are not sufficient to study protection of the average female. Futhermore, for more severe injuries recent studies have shown that females are at higher risk than males of sustaining severe injuries in comparable crashes [25]. This was the driving force behind the development of a 50$^{th}$ percentile female HBM as described in this paper. In addition, the influence of using a detailed and a simplified neck model was investigated.

An Open Source FE HBM of the 50$^{th}$ percentile female was developed, initially for assessment of whiplash protection systems, but also as a platform for the development of a female FE HBM model with the same capabilities as contemporary 50$^{th}$ percentile male FE HBMs.

## II. METHODS

The female HBM (Fig. 1) was created from stereolithography (STL) surfaces[26, 27] of the skeleton and outer surface of a 31 year old female subject of 161.6 cm stature and 60.8 kg weight (within 0.1% and 2% of the target 50$^{th}$ percentile female[16]). Ten more anthropometric measurements (e.g. seated height and hip breadth) were verified to be within 5% of the value for the 50$^{th}$ percentile female [28] for the subject. The STL surfaces were created from a total of 138 scan series with approximately 20,000 images which were captured in an automotive seated posture using several modalities (magnetic resonance imaging, computed tomography and external measurements) [26, 27].

Mesh generation was made with Hypermesh 13.0 (Altair, Troy, MI), pre- and post-processing was done with LS-PrePost (LSTC, Livermore, CA) and Matlab (The Mathworks, Natick, MA). Simulations were run with single and double precision LS-DYNA MPP R8.1.0 (LSTC, Livermore, CA) on Intel Xeon E5-2650V3 cluster machines (10 cores/20 threads). A global coordinate system with X forward, Y to the left and Z upwards was utilised for the model (Fig. 1).

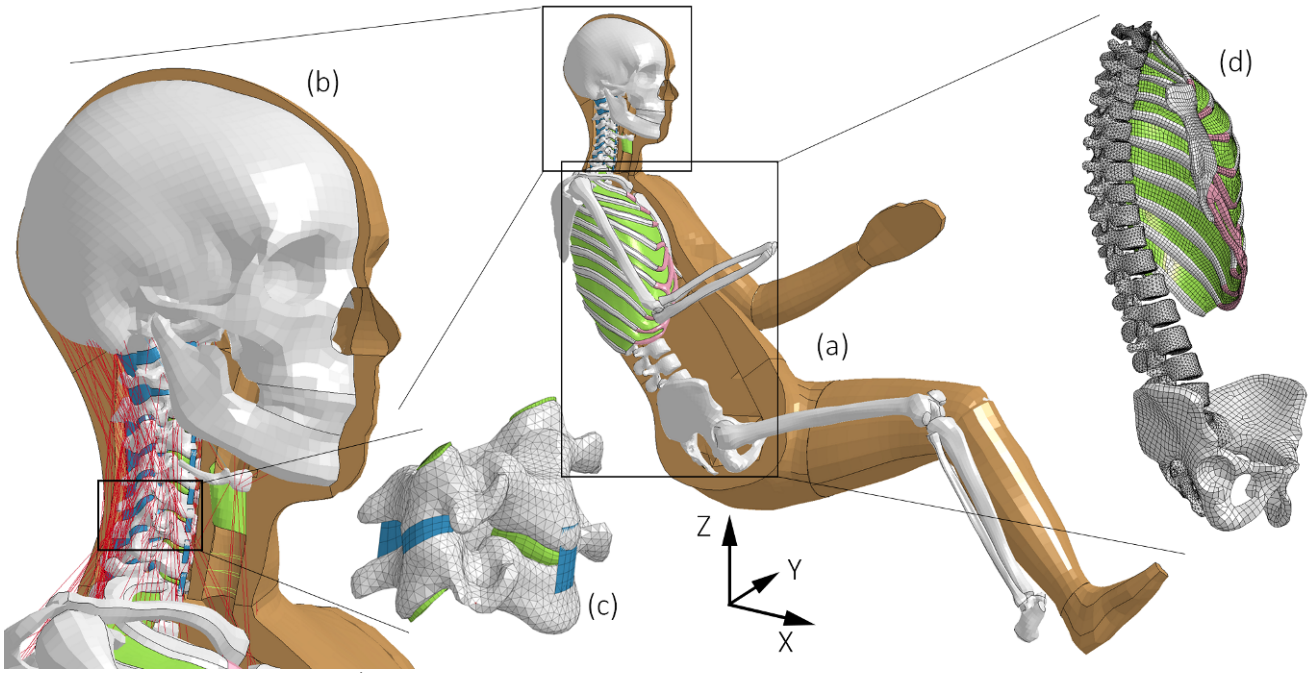


Fig. 1. (a) Overview of the 50$^{th}$ percentile female HBM. (b): close-up view of the cervical spine. (c): the C5C6 vertebral segment. (d): the axial skeleton (to C7 level), pelvis, and left side of the thoracic cage (right side blanked out to reveal the vertebral column).

***Torso***

The torso was modelled as a combination of rigid and deformable bodies. The external soft tissue and skin layer, Fig. 1, was extended continuously from the neck to the superior portion of the femur. The spine, from T1 to sacrum and pelvis, was modelled with rigid bodies, connected with compliant kinematical joints. Six degrees of freedom intervertebral joint properties were based on in vitro studies [29–32]. The ribcage was modelled with rigid costae and sternum, connected by linear elastic hexahedral elements representing the costal cartilage, Fig. 1(d). The costae were connected to each other by the intercostal muscles, modelled with linear elastic quadrilateral shell elements. In addition, the costae were attached to the thoracic vertebrae by spherical joints. The external soft tissues were connected to the skeletal rigid bodies by nodal constraints. The thoracic and abdominal cavities were modelled with tetrahedral elements, separated by a quadrilateral shell representing the diaphragm. Both were assigned the same material as the external soft tissues, except the thoracic cavity which has a lower density calculated based on its volume and an approximate target weight for a female [33]. The density used for the soft tissue bulk of the whole model was 890 kg/m$^3$, chosen to provide a total model weight of 62.3 kg. A summary of the material data used for the torso and extremities, based on experimental data [29–32, 34–39], is found in TABLE I.

TABLE I

SUMMARY OF MATERIAL AND ELEMENT PROPERTIES USED FOR THE FEMALE HBM.

Ref. = References; N/A = Not Applicable; Min. = Minimum; Max. = Maximum; LS-DYNA specific entries: ELFORM = element formulation number; HGID = hourglass formulation number; *MAT_no = material number. †The shoulder and middle of the thigh is modelled with tetrahedral (ELFORM 13) and triangular (ELFORM 4) elements.

| **Part(s)** | **Element type (ELFORM)** | **Characteristic element length (mm)** | **Hourglass control (HGID)** | **Constitutive model (*MAT_no)** | **Material parameters** | **Shell/ beam thickness (mm)** | **Ref.** |
|---|---|---|---|---|---|---|---|
| Skin, whole model | Quadrilateral membrane (9†) | Min. = 2.2<br>Median=13.6<br>Max. = 66.6 | N/A | Linear elastic (001) | E=1 MPa<br>v=0.40<br>ρ=1000 kg/m$^3$ | 1 mm | [35] |
| Extremity soft tissues | Hexahedral (1†) | Min. = 1.5<br>Median = 6.1<br>Max. = 64.8 | Viscous (3) | Ogden rubber (077_O) | ρ=890 kg/m$^3$<br>v=0.4999<br>$\mu_1$=0.318 MPa<br>$\mu_2$=−0.401 MPa<br>$\alpha_1$=1.492<br>$\alpha_2$=-3.316<br>$G_1$=0.235 MPa<br>$B_1$=100 s$^{-1}$<br>… | N/A | [39] |
| Soft tissues, torso | Hexahedral (1†) | Min. = 1.2<br>Median =8.3<br>Max. = 70.8 | Stiffness based (5) | Ogden rubber (077_O) | ρ=890 kg/m$^3$<br>v=0.4999<br>$\mu_1$=30 Pa<br>$\alpha_1$=20<br>$G_1$=3 kPa<br>$B_1$=310 s$^{-1}$ | N/A | [36] |
| Abdominal cavity | Tetrahedral (13) | Min. = 3.6<br>Median = 13.1<br>Max. = 50.2 | N/A | Ogden rubber (077_O) | Same as above. | N/A | [36] |
| Thoracic cavity | Tetrahedral (13) | Min. = 6.5<br>Median = 20.2<br>Max. = 60.7 | N/A | Ogden rubber (077_O) | ρ=270 kg/m$^3$<br>Same as above | N/A | [36] |
| Intercostal muscles | Quadrilateral shell (2) | Min. = 0.9<br>Median = 3.7<br>Max. = 8.0 | Viscous (3) | Linear elastic (001) | E=1.03 MPa<br>v=0.49<br>ρ=1000 kg/m$^3$ | 0.5 mm | [37] |
| Diaphragm | Quadrilateral shell (2) | Min. = 12.0<br>Median = 17.6<br>Max. = 37.1 | Viscous (3) | Linear elastic (001) | Same as above | Same as above | [37] |
| Costal cartilage | Hexahedral (1) | Min. = 0.7<br>Median = 2.5<br>Max. = 16.1 | Viscous (3) | Linear elastic (001) | E=22 MPa<br>v=0.49<br>ρ=1000 kg/m$^3$ | N/A | [38] |
| Thoracolumbar intervertebral joints | Beam(Discrete beam) (6) | N/A | N/A | 6 DOF Discrete beam (119) | Tabulated curves from references | N/A | [29–32] |

TABLE I CONTINUED

| | | | | | | |
|---|---|---|---|---|---|---|
| Costovertebral joints | Spherical joint *CONSTRAINED_JOINT_SPHERICAL | | 3 DOF joint stiffness *CONSTRAINED_JOINT_STIFFNESS_GENERALIZED | Tabulated curves from reference | N/A | [34] |
| Torso and extremity cortical bone | Quadrilateral and triangular shell (2 and 4) | Min. = 0.6<br>Median = 3.5<br>Max. = 18.1 | N/A | Rigid (020) | ρ=2000 kg/m$^3$ | 0.53–4.8 mm |
| Torso and extremity trabecular bone | Hexahedral and tetrahedral (1 and 13) | Min. = 0.4<br>Median = 2.6<br>Max. = 18.5 | N/A | Rigid (020) | ρ=1000 kg/m3 | N/A |

***Extremities***

The bones of the upper and lower extremities were modelled as rigid bodies and soft tissues with hexahedral solid elements, connected to the bones by nodal constraints. For the sake of computational stability, a stiffer material was chosen for the soft tissues of the extremities; a rubber material representative of the elastomer of the Hybrid III head was used [39]. The joints were modelled as spherical, saddle or revolute joints, with a range of motion based on literature reports from in-vivo studies or estimated, TABLE II. A resistance of 1 Nm over the range of motion has been included for each joint. The scapulothoracic joint, which has a relatively complex motion pattern, was simplified to a spherical joint, with a resistance of 10 Nm/rad for all rotations, connecting the scapula to the fifth rib. This was deemed sufficient for the purpose of simulating whole body impact kinematics in the sagittal plane; it should be noted that it likely affects the response in side impacts to the shoulder. The scapulae and claviculae were also connected to the torso soft tissue by nodal constraint of overlapping nodes.

TABLE II

RANGE OF MOTION FOR THE UPPER AND LOWER EXTREMITY JOINTS.

| Joint | Joint type | Movement | Range of Motion (°) | Reference |
|---|---|---|---|---|
| Hip | Spherical | Flexion-Extension | 144 | [40] |
| | | Abduction-Adduction | 77 | [40] |
| | | External-Internal rotation | 67 | [40] |
| Knee | Revolute | Flexion-Extension | 134 | [40] |
| Sternoclavicular | Saddle | Elevation-Depression | 36 | [41] |
| | | Protraction-Rotation | 30 | [41] |
| Scapulothoracic | Spherical | X rotation* | 60 | Estimated |
| | | Y rotation* | 35 | Estimated |
| | | Z rotation* | 20 | Estimated |
| Glenohumeral | Spherical | Flexion-Extension | 165 | [42] |
| | | Abduction-Adduction | 90 | [42] |
| | | Rotation | 135 | Estimated |
| Humeroulnar | Revolute | Flexion-Extension | 105 | [43] |

*In a local scapula coordinate system with origin at the trigonum scapulae; the X-axis pointing towards the angulus inferior; Z in the plane formed by these points and the angulus acromialis; and Y perpendicular to X and Z.

***Head and Neck***

The cervical spine has previously been described and validated for quasistatic loading on both segment and whole ligamentous spine level [44], as well as in dynamic rear-impact simulations [45]. It consists of a rigid body head, linear elastic vertebrae modelled with tetrahedral and triangular elements, intervertebral discs modelled as composites of hexahedral bulk elements and orthotropic membranes, intervertebral ligaments modelled with orthotropic non-linear elastic membranes, line muscle elements, and sliding contacts for the facet joint, Fig. 1 (b) and (c). For the present study, a simplified neck model was developed. For this simplified model the intervertebral soft tissue structures were removed and kinematic compliant joints were implemented at the instantaneous centres of rotation [45] for each vertebral joint of the model. Translational intervertebral joint compliance [46], axial rotation and lateral bending [47] and flexion–extension compliance [48] were implemented based on in-vitro data from human subjects. Contacts between vertebrae were also included in the simplified model.

***Simulations***

Simulations of three Post Mortem Human Subject (PMHS) tests, TABLE III, were conducted in order to validate the kinematic response of the whole body HBM in three principal directions; frontal [49, 50], lateral/roll-over [51], and rear [52]. The simulations were run with the HBM with the detailed and the simplified neck model. For these simulations, a 500 ms pre-simulation for positioning and settling was included. During this time the hands of the model were moved to the lap, and global damping was included to remove kinetic energy related to the positioning. The seat belt was modelled as a combination of 1D and 2D seat belt elements, with linear elastic material properties (w=47 mm, t=1.25 mm, E=2.48 GPa). The whole body simulations were run with a double precision binary as the total number of cycles exceeded $10^6$. Furthermore, no muscle activation was used in any of the simulations.

TABLE III

PMHS AND HBM ANTHROPOMETRIC MEASUREMENTS AND SCALING FACTORS.

n = Number of subjects. N/A = Not Applicable.

*Sitting height for North American subjects of the same stature in the DINED anthropometric database [53].

| Load Case / HBM | Reference | Sex | Mean Stature (cm) | Mean Weight (kg) | Sitting Height* (mm) | Displacement scale factor $R_d$ | Force scale factor $R_F$ |
|---|---|---|---|---|---|---|---|
| Frontal Impact | [49, 50] | Male, n=8 | 179.4 | 75.5 | 930 | 0.929 | 0.825 |
| Roll-over | [51] | Male, n=4 | 180.2 | 80.4 | 936 | 0.931 | 0.775 |
| Rear-impact | [52] | Female, n=1 | 156 | 55.4 | 835 | 1.035 | 1.124 |
| HBM | N/A | Female | 161.6 | 62.3 | 864 | N/A | N/A |

*Frontal Impact*

Shaw *et al*.[49] tested eight male PMHSs, TABLE III, in a 40 km/h frontal impact test on a rigid seat with a custom three-point seat belt. To model this test, the HBM was rotated +10° around the Y-axis during pre-processing to match the average PMHS sternum angle of 22 ° (Fig. 2a) and the upper attachment for the shoulder belt was adjusted 110 mm downward to achieve a seat belt angle of 27°, similar to the mean for the PMHSs[49]. The knee bolster and foot rest were not modelled, instead the knee support was replaced with 200 N/mm springs connecting the patellae to the buck (with the stiffness based on the force-displacement response of the PMHS in Shaw et al. [49]).

*Lateral/Roll-over*

Lessley *et al*.[51] tested four male PMHSs, TABLE III, repeatedly in different roll-over combinations. For the present study, the pure dynamic roll-over over one full revolution at average rotational velocity of 260°/s and a peak resultant acceleration of 33 $m/s^2$ was simulated. Part of the test buck [54] was modelled (Fig. 3a). The HBM was rotated +15° around the Y-axis during pre-processing to match the angle of the block supports (15° from the vertical). The feet and proximal tibia were secured to the buck using point constraints, as a simplified model of the aluminium footrest and ankle straps used in the experimental setup [51]. Displacement data for this simulation were presented in a coordinate system that rotates with the buck (X forward, Y to the left, Z upward at the initial position, roll angle $\varphi$=0°).

*Rear-impact*

Several rear-impact studies with PMHS have been conducted, e.g. [52,55–58]. However, most publications do not contain detailed kinematic data similar to the more recent frontal impact [49] and roll-over [51] experiments. For the present work, the test of Yoganandan *et al*. [52], which was performed with a rigid seat without a head rest and with female PMHSs was simulated. The rigid seat and custom three-point seat belt were modelled (Fig. 2e) and the HBM was rotated by 11.5° during pre-processing. The feet were supported by contact with a floor plate, but otherwise unconstrained. Moreover, simulations with two additional cervical spine postures were conducted (Appendix B). For these simulations, the head was moved 20 mm rearward or forward of the position described previously, and the T1 vertebra 10 mm forward or rearward.

*Isolated Head-Neck Impacts*

To compare the detailed and simplified neck model responses, six additional simulations with the isolated head and neck of the HBM were made to represent generic frontal, lateral, and rear-impacts. In these, the distal end of the cervical muscles and soft tissue were constrained to move with the T1 vertebra using nodal constraints. After a settling simulation of 100 ms with global damping, a sine-shape pulse with peak acceleration of 47 $m/s^2$ and duration of 0.1 s ($\Delta V=3 m/s^2$) was applied to the T1 vertebra in positive X, positive Y, and negative

X directions. Simulations were run with a single precision binary, with both the detailed and simplified neck models. The movement of the geometric centres of the T1–C2 vertebral bodies were tracked, as well as the head Centre of Gravity (CG) and Occipital Condyles (OC) locations. Relative intervertebral rotations between each spinal segment were also evaluated.

***Scaling and Objective Rating***

For impact biomechanics testing, significant variation in subject size, shape and weight is usual. To reduce the variation in testing, scaling of response data to a target anthropometry is common; a typical approach is using a mechanical analogue [59] as a basis for a scaling law. For the present work the male subject data [49–51] was scaled to 50$^{th}$ percentile female size using an inverted pendulum analogue [45, 60] so that:

$$X_{F50}=R_d*X_{PMHS} \text{ and } F_{F50}=R_F*F_{PMHS} \quad (1), (2)$$

Here, X is a displacement, $R_d$ the displacement scale factor, F a force, and $R_F$ the force scale factor according to:

$$R_d=SH_{F50}/SH_{PMHS} \text{ and } R_F=M_{F50}/M_{PMHS} \quad (3), (4)$$

where SH is the sitting height of the subjects, and M is the total body mass, according to TABLE III. The sacrum displacements were not scaled, based on the assumption that the pelvis mainly undergoes translation during events simulated. The female subject data for the rear-impact test case was not scaled either.

Objective rating of the kinematic responses was made using the Correlation Analysis (CORA) software 3.6.1 (PDB, Gaimersheim, Germany). CORA provides a rating between 0 and 1 for the similarity of a signal to reference data, considering both a corridor fit and cross-correlation of the signal to the reference [61]. For the frontal impact and roll-over load cases, the inner corridors were selected as +/- 1 Standard Deviation (SD) corridors, and the outer corridors as +/- 2 SD. For the rear-impact load case the CORA default corridors of 5% and 50% of the peak value for the inner and outer corridor, respectively, were used. Equal weights were used in the calculation of all total rating values.

## III. RESULTS

The HBM consisted of 318,400 elements; with the simplified neck the total number of elements was 306,000. A mesh quality assessment showed that 95% of all elements had an aspect ratio of < 3 (maximum 13.8), 90% of the solid and 97% of the shell elements had Jacobian values > 0.7, while 99.9% of all elements had Jacobian values > 0.4. For the simulations with the HBM with detailed neck, the CPU time per ms simulation time was 54 s/ms, 56 s/ms, and 50 s/ms, for the frontal impact, lateral/roll-over, and rear-impact simulations, respectively. For the corresponding simulations with the simplified neck, the CPU time was reduced by 39% for all cases. The frontal impact simulations (Fig. 2(a–d)) involving the HBM with both the detailed and the simplified neck, completed 150 ms of the impact simulation. The roll-over simulation with the detailed neck (Fig. 3) terminated after 1,183 ms and 314° roll angle due to negative volume in a hexahedral articular cartilage element at the right C3C4 facet joint. The roll-over simulations with the simplified neck completed the full simulation. In the rear-impact simulation (Fig. 2(e–h)) both models completed the full simulation.

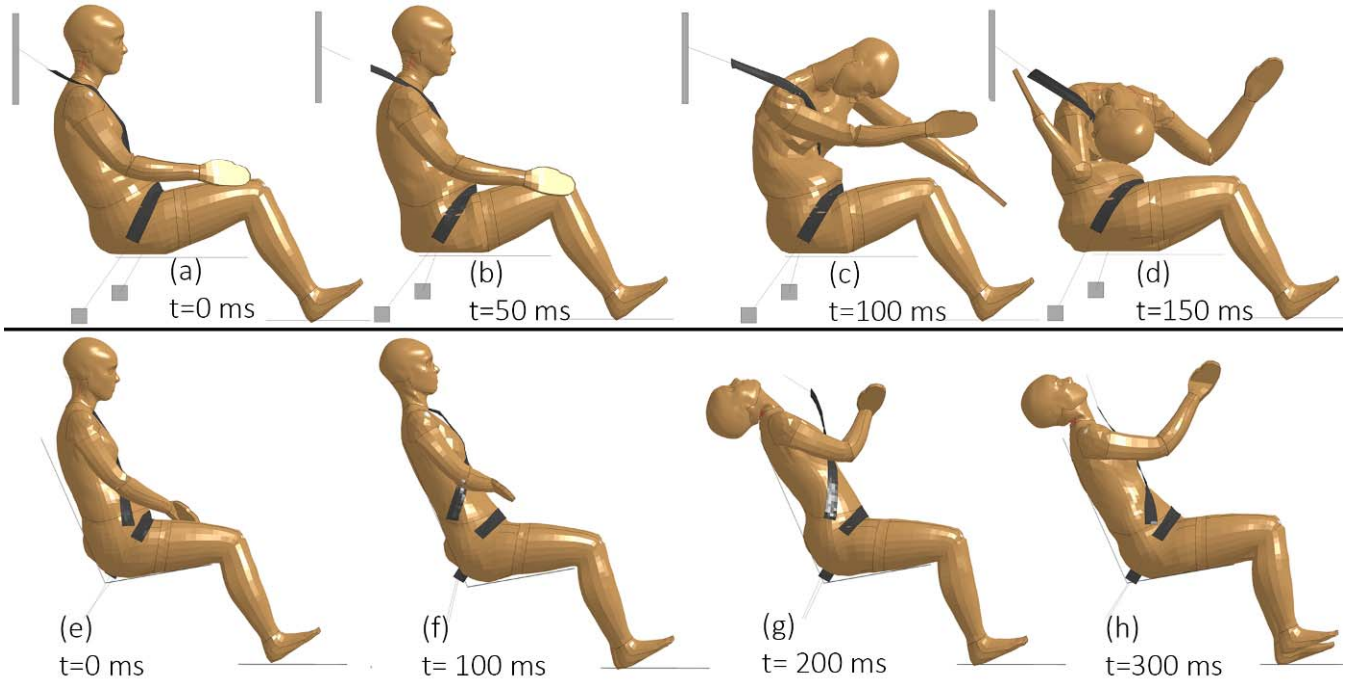


Fig. 2. (a)–(d): Time-series of the frontal impact simulation; and (e)–(h): Time-series of the rear-impact simulation.

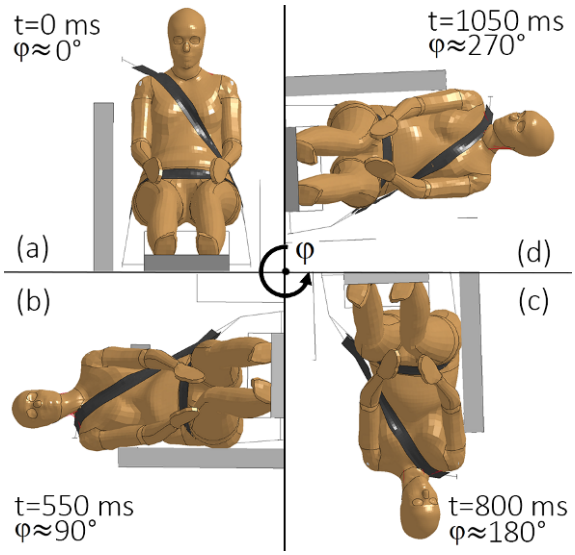


Fig. 3. Time-series of the roll-over simulation: (a): initial posture of the model at the beginning of the event. (b)–(d): model kinematic response at approximately 90°, 180° and 270° roll angles φ.

*Frontal Impact*

Head and T1 kinematic responses for the three whole body simulations are presented in Fig. 4–6. The additional kinematic responses for lower spinal levels and the shoulders, as well as seat belt force responses, are available in Appendix A (Fig. A1–A6). For the frontal impact scenario, the correlation of both HBMs with respect to the scaled PMHS data was good, with both Head and T1 X-displacement responses inside the scaled PMHS corridor. However, the Y-displacements were on the boundary or just outside the corridor, and the Z-displacements were mostly outside the corridors. The overall correlations of all kinematic responses in the X-direction, which was the principal direction for the frontal impact load case, were 0.91 and 0.92, while the grand total correlations for the frontal impact load case were 0.76 and 0.78 for the HBM with the detailed and with the simplified neck, respectively (TABLE IV).

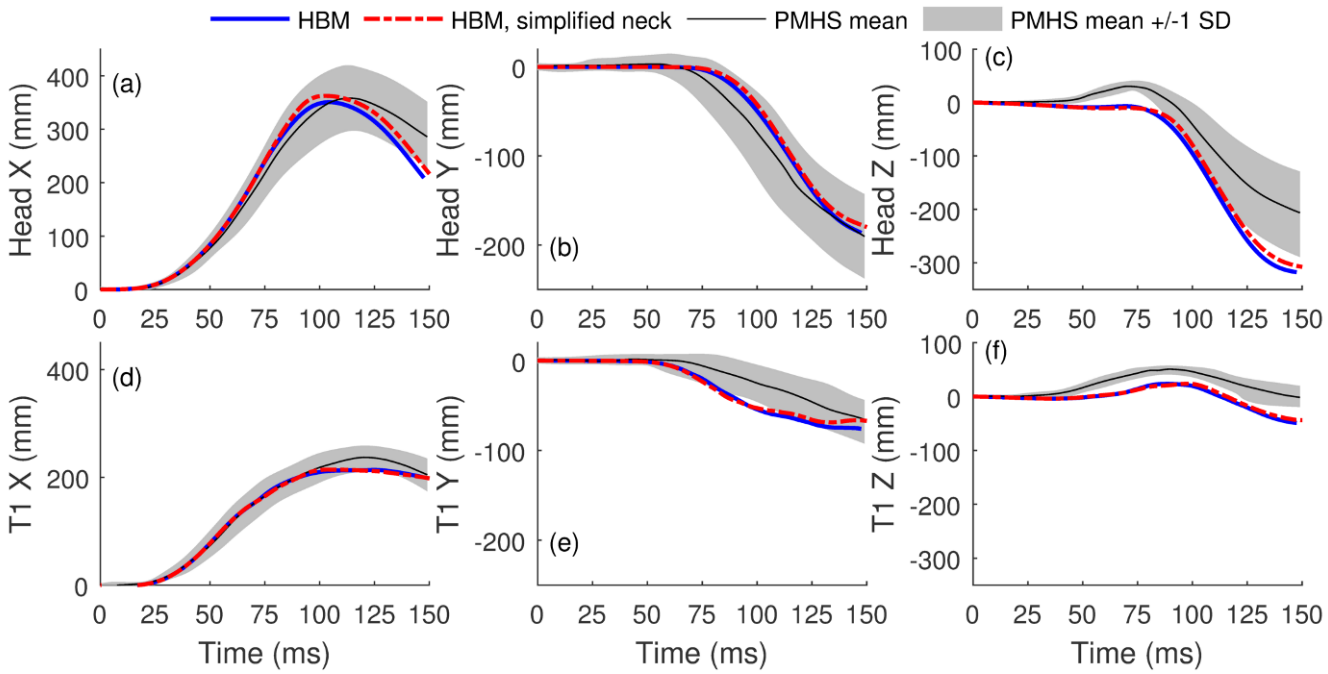


Fig. 4. Head and T1 kinematics of the HBM in the frontal impact simulations, compared with that of scaled PMHS data [49, 50]. SD = Standard Deviation.

TABLE IV

OBJECTIVE RATING RESULTS OF WHOLE BODY SIMULATIONS.

The shaded columns represent the primary kinematics variable in each of the load cases. Total is the weighted [61] sum of each column, while the grand total for each load case is the weighted sum of each total for the load case.

| **HBM with detailed neck** | | | | | | | | | |
|---|---|---|---|---|---|---|---|---|---|
| | **Frontal Impact** | | | **Roll-over** | | | **Rear-impact** | | |
| | X | Y | Z | X | Y | Z | X | Y-rotation | Z |
| Head | 0.94 | 0.97 | 0.62 | 0.35 | 0.66 | 0.28 | 0.70 | 0.76 | 0.29 |
| T1 | 0.97 | 0.81 | 0.24 | 0.48 | 0.77 | 0.43 | 0.78 | 0.59 | 0.30 |
| T4/T8 | 0.97 | 0.88 | 0.65 | 0.57 | 0.75 | 0.46 | | | |
| T10/L2 | 0.80 | 0.71 | 0.86 | 0.63 | 0.50 | 0.45 | | | |
| L1/L4 | 0.84 | 0.71 | 0.88 | 0.29 | 0.63 | 0.41 | | | |
| Sacrum | 0.93 | 0.80 | 0.80 | 0.32 | 0.91 | 0.95 | 0.41 | 0.25 | 0.36 |
| Left Shoulder | 0.99 | 0.95 | 0.41 | 0.40 | 0.53 | 0.32 | | | |
| Right Shoulder | 0.82 | 0.64 | 0.20 | 0.20 | 0.62 | 0.26 | | | |
| Total | **0.91** | 0.81 | 0.58 | 0.40 | **0.67** | 0.45 | **0.63** | **0.53** | 0.31 |
| Grand total | 0.76 | | | 0.51 | | | 0.49 | | |
| **HBM with simplified neck** | | | | | | | | | |
| Total | **0.92** | 0.79 | 0.63 | 0.42 | **0.67** | 0.38 | **0.63** | **0.54** | 0.33 |
| Grand total | 0.78 | | | 0.49 | | | 0.50 | | |

*Lateral/Roll-over*

In the roll-over load case, both HBMs showed an exaggerated oscillatory response in the Head X-displacement compared with the scaled PMHS data, Fig. 5(a). This appeared to be due to a difference in the initial head CG location, which gave an initial forward movement in the HBM, causing subsequent oscillatory axial rotation of the head. The principal direction for the load case was Y-displacement, and the overall correlation in this direction is 0.67 for both models, while the grand total for the load case was 0.51 and 0.49, respectively, for the HBM with the detailed and with the simplified neck (TABLE IV). For the Z-displacement, the head moved more upward than for the PMHS initially, and for both the head and T1 the subsequent downward movement was smaller than for the PMHS.

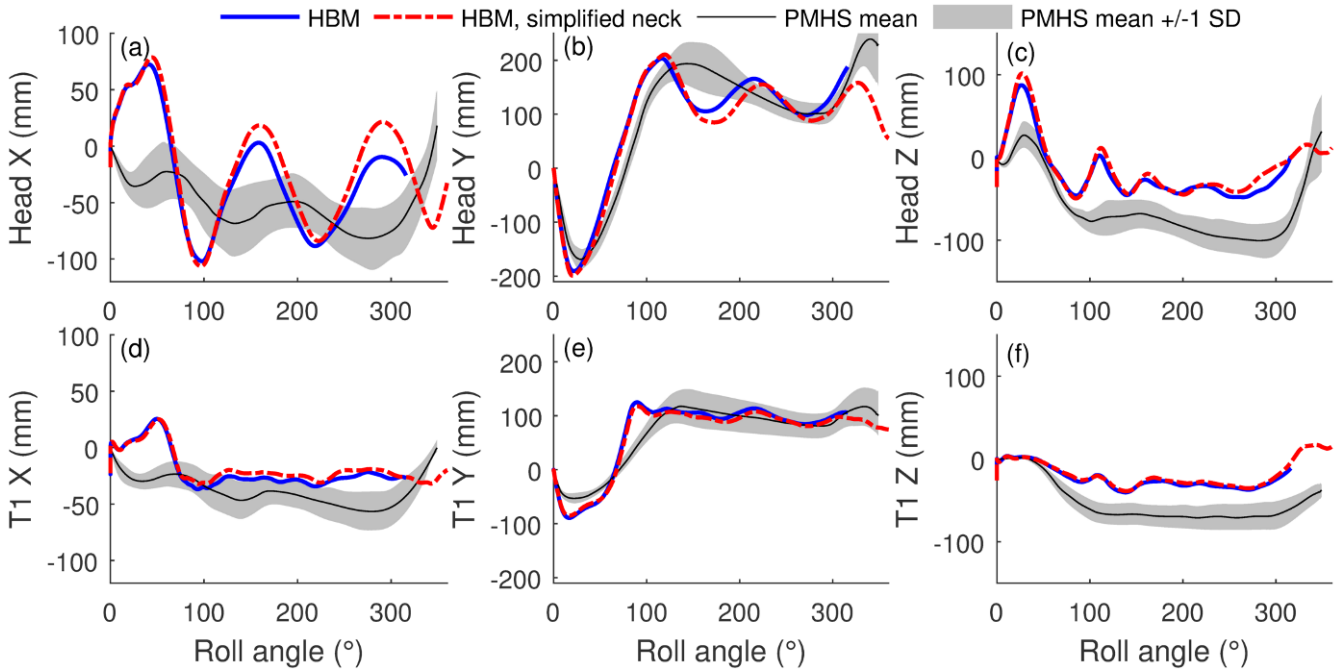


Fig. 5. Head and T1 kinematics of the HBM relative to the buck roll-angle in the roll-over simulations, compared with that of scaled PMHS data [51]. SD = Standard Deviation.

*Rear-impact*

In the rear-impact load case (Fig. 6) the HBM showed the same general kinematics as the female PMHS included for comparison, but the peak head displacement and rotation were smaller. The T1 displacements matched well, but this was largely due to the positioning of the model, i.e. the distance between the seat back and T1 at time 0. The HBM showed less upward movement of the head, which was likely an effect of different initial cervical posture between model and PMHS (Appendix B). The correlation in the principal direction for the load case, X, was 0.63 for both models, and the grand total was 0.53 and 0.54, respectively, for the HBM with the detailed and simplified neck, TABLE IV.

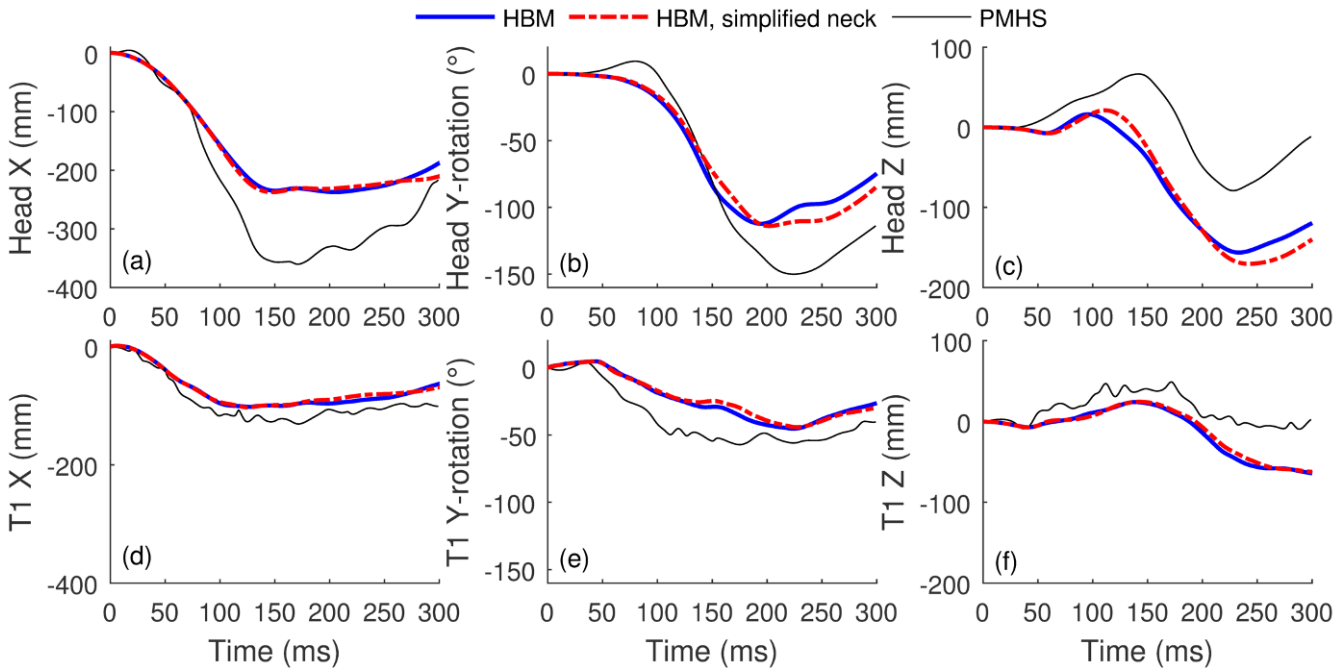


Fig. 6. Head and T1 kinematics in the rear-impact simulations, compared with that of one female PMHS [52].

*Isolated Head-Neck Impacts*

All the isolated head-neck simulations reached the termination time of 0.2 s, except the lateral impact with the simplified neck. The simplified neck model had a 63% shorter simulation time than the detailed model (7 s/ms compared with 19 s/ms) for all simulations. The head CG trajectory and spinal curvature (Fig. 7) qualitatively revealed a large difference in kinematic response between the two models. For the model with the simplified neck, the head was more loosely coupled to T1 and lagged behind in the impact more than for the detailed neck, for which the head CG had a more arched movement.

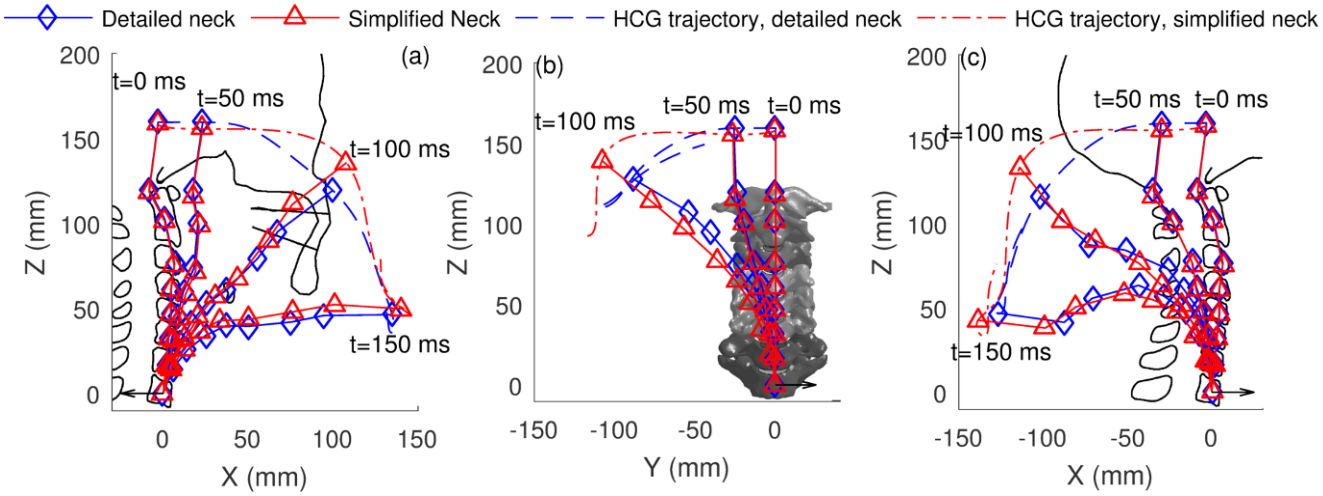


Fig. 7. Cervical spine curvature and Head Centre of Gravity (HCG) trajectories in 47 m/s$^2$ isolated head-neck impact simulations: (a): frontal impact. (b): lateral impact. (c): rear-impact. The markers indicate the geometric centres of the T1–C2 vertebrae, the Occipital Condyles (OC) and HCG location relative to the T1 vertebra. The arrows at the T1 centre indicate the movement direction of T1 in the simulation. The images in the background represent the cervical spine in the initial posture at t=0 ms.

For all loading directions, there was an S-shaped deformation of the cervical spine, which was manifested in the Upper Cervical Spine (UCS) segment rotations being opposite to the Lower Cervical Spine (LCS) segment rotations up until about 0.1 s into the event (Fig. 8). For example, in the lateral impact the C2–C3 segment and above were in left bending while the T1–C3 segments were all in right bending for the first 0.1 s of the event. Compared with the HCG trajectory data (Fig. 7) the difference between models in relative intervertebral rotations (Fig. 8) was not as apparent.

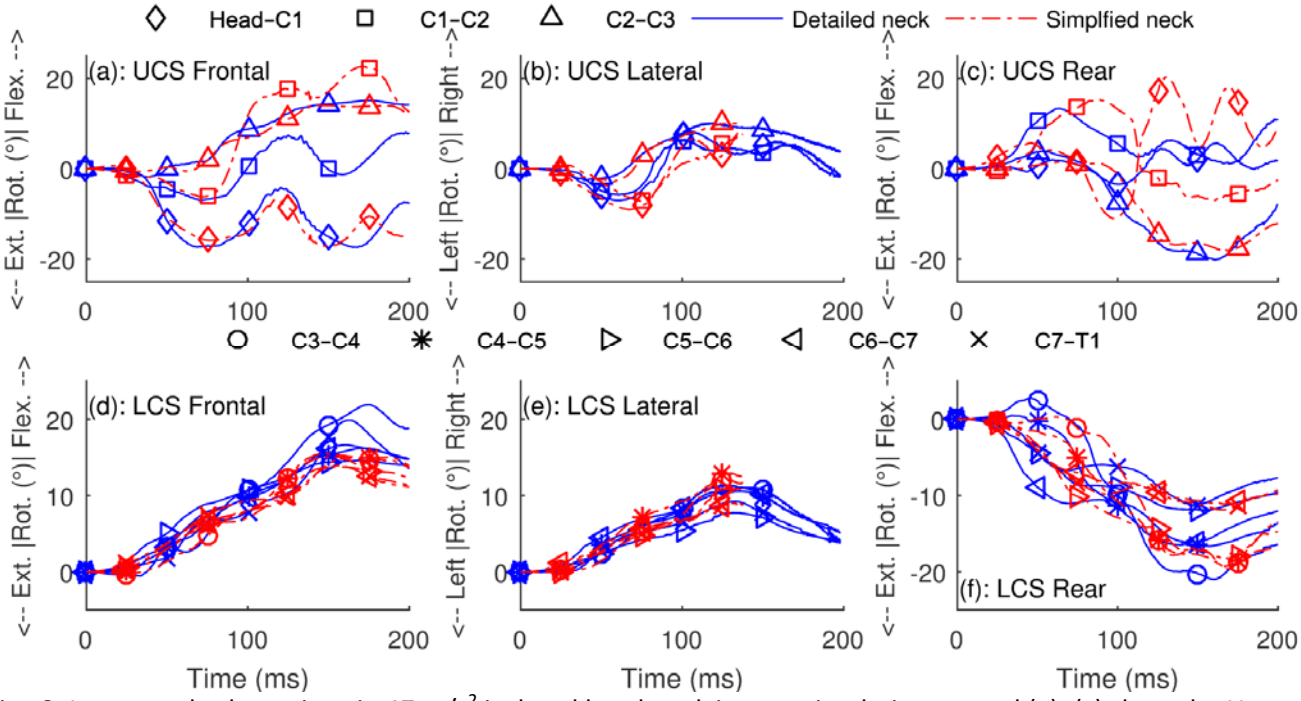


Fig. 8. Intervertebral rotations in 47 m/s$^2$ isolated head-neck impact simulations: panel (a)–(c) show the Upper Cervical Spine (UCS) segments C2–C3, C2–C1, and C1–Head; (d)–(f) show the Lower Cervical Spine (LCS) segments T1–C7, C7–C6, C6–C5, C5–C4, and C4–C3. Ext. = Extension; Flex. = Flexion; Rot. = Rotation.

## IV. Discussion

In this paper, a simplified whole body 50$^{th}$ percentile female FE HBM with a detailed neck model was developed and its kinematics were validated in frontal, lateral, and rear impacts. This work was motivated by the fact that the average female has not been addressed by other contemporary FE HBM projects, such as the THUMS or the GHBMC [8–12]. Some previous studies have targeted the 50$^{th}$ percentile female, but these have had to start their work with scaling models, either from a 5$^{th}$ percentile female [62] or from a 50$^{th}$ percentile male model [63]. Geometric scaling of the average male is problematic as there are several systematic morphological differences between males and females that are not accounted for, e.g. in the cervical spine [64]. State-of-the-art approaches for scaling applying morphing [10, 65] with a large number of target points could possibly account for some of these morphological differences. However, it would seem more reasonable to begin morphing female models from a 50$^{th}$ percentile female as developed here rather than existing 5$^{th}$ percentile female models or 50$^{th}$ percentile male models; ideally, possible dimorphic differences in mechanical tissue properties [66, 67] would then also be accounted for. For example, if one would be interested in 25$^{th}$, 75$^{th}$, or 95$^{th}$ percentile female model, or to make population based studies with morphed female models, a 50$^{th}$ female HBM would be a much better starting point than a 50$^{th}$ percentile male model or the outlier 5$^{th}$ female.

The validation of the model revealed that for the frontal impact condition, the model correlates well with the scaled male PMHS data. Davis *et al*. [10] performed a validation of a state-of-the-art 5$^{th}$ percentile female model with respect to the same PMHS data set [49], but in contrast to the present study they morphed the 5$^{th}$ percentile HBM to PMHS size and also scaled the HBM response data rather than scaling the PMHS data. Objective rating was not carried out in the same way in both studies, but it appears that the model developed here was slightly better correlated for the frontal impact load case with respect to the kinematic response than the morphed 5$^{th}$ percentile model [10]. Both the present work on an average female, and the development of a small female [10], would benefit from studies including female PMHS data of similar level of detail [49, 51] as the impacts simulated here. In the lateral/roll-over simulation the correlation was lower. However, in the Y direction which is the direction of principal interest for this simulation, it was 0.67, which can be deemed as fair. The rear case has the lowest correlation, 0.63 in the principal direction, a low number of kinematic measures included, and only one subject for comparison in the evaluation. As one of the aims for the model is to use it for rear-impact assessment, this is unsatisfactory. However, it should be noted that the head and neck of the model have been validated in more detail for this impact direction [45], and that additional validations will be made for comparison to volunteer test data after including postural and reflexive control[68–70] in the HBM.

Moreover, CORA [61] was used for comparison with the single PMHS in the rear-impact load case, even though it would make more sense to do a direct curve to curve comparison using cross-correlation. This is included as a subset of CORA and to be consistent with the other two load cases CORA was used also for this single specimen comparison.

A few issues with numerical stability of the model were revealed. This was expected in the frontal impact simulation, which is quite severe. For the lateral/roll-over simulation, which is challenging with regard to its duration of 2,000 ms, the detailed cervical spine models contact at the facet joints caused the termination. Addressing these issues is challenging, and appears to have been customarily handled by increasing the elastic stiffness of HBMs producing a response that is too stiff at low loads [69, 70].

For the present study, a simplified neck model was also developed for the HBM. The simplified neck significantly reduced the computational time for the whole body simulations, but it influenced the total and grand total model correlation with respect to the PMHS data only marginally. The reason for this is that the difference between detailed and simplified neck response, even though clear at the isolated neck level, only provides a small change in the whole body CORA rating. Therefore, a simplified modelling approach seems justified if the detailed structural response of the cervical spine is not of importance. Modelling the cervical spine with kinematical joints has been done in previous head-neck FE models [71], but less frequently for more contemporary models. The comparison between the detailed and the simplified head-neck model shows that at least for the present simplified neck implementation a clear difference in the detailed head kinematic response is found. This indicates that for precise head-neck kinematics predictions a detailed model is needed (which is also the model version that is validated with respect to PMHS data in rear-impact [45]).

In the present work, the 50$^{th}$ percentile female HBM has been validated with reasonable responses in three different impact directions. Upcoming steps planned in the development of the model are to include active musculature with feedback postural and reflexive control [68, 70], to validate the HBM's response with respect to rear impact volunteer data, and to establish injury criteria for soft tissue injuries of the cervical spine. In addition, the model can be improved in several areas for which simplified modelling approaches have been used; deformable costae and more detailed internal organs would increase the biofidelity of the model for a wider range of loading scenarios than assessed here (e.g. submarining loading). As the model is developed under an Open Source license, other researchers are encouraged to download, use and further develop the model. Download it at:
http://www.chalmers.se/en/projects/Pages/OpenHBM.aspx. A brief user manual for the HBM is included in Appendix C to this paper.

## V. CONCLUSIONS

A simplified whole body 50$^{th}$ percentile female FE HBM with a detailed neck model was developed and validated with respect to its kinematics in frontal, lateral, and rear-impacts. The model compared well with respect to scaled male and female PMHS data. Both a detailed and a simplified neck model with kinematic joints were used in the validation simulations. Using a simplified neck model influenced the correlation only marginally in whole body simulations, while in isolated-head neck simulations the head kinematics was affected.

## VI. ACKNOWLEDGEMENTS

This study was funded by VINNOVA – Swedish Governmental Agency for Innovation Systems (grant no. 2013-03095), carried out at SAFER–Vehicle and Traffic Safety Centre at Chalmers, and simulations were performed on resources at Chalmers Centre for Computational Science and Engineering (C3SE) provided by the Swedish National Infrastructure for Computing (SNIC). The authors acknowledge Elemance, LLC. (Winston-Salem, NC) for STL surface geometry development in support of this project. Lastly, the authors would like to thank Elisabet Agar for language editing of the manuscript.

## VII. REFERENCES

[1] Yang KH, Hu J, White NA, King AI (2006) Development of Numerical Models for Injury Biomechanics Research: A Review of 50 Years of Publications in the Stapp Car Crash Conference. *Stapp Car Crash Journal*, **50**: pp. 429–90.

[2] Iwamoto M, Kisanuki Y, Watanabe I, Furusu K, Miki K (2002) Development of a Finite Element Model of the Total Human Model for Safety (THUMS) and Application to Injury Reconstruction. *Proceedings of the IRCOBI Conference*, 2002, Munich, Germany.
[3] Robin S (2001) Humos: Human Model for Safety – A Joint Effort Towards the Development of Refined Human-like Car Occupant Models. *Proceedings of the 17th ESV Conference*, 2001, Amsterdam, The Netherlands.
[4] Hartlieb M. *et al.* (2015). Implementation of New Rib Material Models to a FE-Human Body Model for Evaluation of the Pre-Safe Impulse Side Restraint System for Side Impact Protection. *Proceedings of the 24th ESV Conference*, 2015, Gothenburg, Sweden.
[5] Bostrom O, Motozawa Y, Oda S, Ito Y, Mroz K (2013) Mechanism of Reducing Thoracic Deflections and Rib Strain using Supplemental Shoulder Belts during Frontal Impacts. *Proceedings of the ESV 23rd Conference*, 2013, Seoul, Republic of Korea.
[6] Pipkorn B *et al.* (2016) Assessment of an Innovative Seat Belt with Independent Control of the Shoulder and Lap Portions using THOR tests, the THUMS model, and PMHS tests. *Traffic Injury Prevention*, 2016, **17**(S1): pp. 124–30.
[7] Shaw G, Crandall J, Butcher J (2000) Biofidelity Evaluation of the THOR Advanced Frontal Crash Test Dummy. *Proceedings of the IRCOBI Conference*, 2000, Montpellier, France.
[8] Park G, Kim T, Crandall JR, Arregui-Dalmases C, Luzon-Narro J (2013) Comparison of Kinematics of GHBMC to PMHS on the Side Impact Condition. *Proceedings of the IRCOBI Conference*, 2013, Gothenburg, Sweden.
[9] Cronin D, Fice J, DeWit J, Moulton J (2012) Upper Cervical Spine Kinematic Response and Injury Prediction. *Proceedings of the IRCOBI Conference*, 2012, Dublin, Ireland.
[10] Davis ML, Koya B, Schap JM, Gayzik FS (2016) Development and Full Body Validation of a 5th Percentile Female Finite Element Model. *Stapp Car Crash Journal*, 2016, **60**: pp. 509–44.
[11] Vavalle NA, Schoell SL, Weaver AA, Stitzel JD, Gayzik FS (2014) Application of Radial Basis Function Methods in the Development of a 95th Percentile Male Seated FEA Model. Stapp Car Crash Journal, 2014, **58:** pp. 361–84.
[12] Watanabe R, Katsuhara T, Miyazaki H, Kitagawa Y, Yasuki T. Research of the Relationship of Pedestrian Injury to Collision Speed, Car-type, Impact Location and Pedestrian Sizes using Human FE model (THUMS Version 4). *Stapp Car Crash Journal*, 2012, 56: 269–321.
[13] van Ratingen MR (2016) Saving Lives with Safer Cars: The Past, Present, and Future of Consumer Safety Ratings. *Proceedings of the IRCOBI Conference*, 2016, Malaga, Spain.
[14] Free Software Foundation. "*GNU General Public License*" Internet: [https://www.gnu.org/licenses/gpl-3.0.html] (Accessed 21 November 2016).
[15] Pheasant S, Haslegrave CM (2006) *Bodyspace – Anthropometry, Ergonomics, and the Design of Work, third edition*. *Taylor & Francis*, London, UK, 2006.
[16] Schneider LW, Robbins DH, Pflüg MA, Snyder RG (1983) University of Michigan Transportation Research Institute *, Development of anthropometrically based design specifications for an advanced adult anthropomorphic dummy family, Final Report*, Ann Arbor, MI.
[17] Kullgren A, Stigson H, Krafft M (2013) Development of Whiplash Associated Disorders for Male and Female Car Occupants in Cars Launched Since the 80s in Different Impact Directions. *Proceedings of the IRCOBI Conference*, 2013, Gothenburg, Sweden.
[18] Carlsson A *et al.* (2014) Anthropometric Specifications, Development, and Evaluation of EvaRID – A 50th Percentile Female Rear Impact Finite Element Dummy Model. *Traffic Injury Prevention*, 2014, **15**: pp. 855–65.
[19] O'Neill B, Haddon W Jr, Kelley AB Sorenson WW (1972) Automobile Head Restraints: Frequency of Neck Injury Claims in Relation to the Presence of Head Restraints. *American Journal of Public Health*, 1972, **62**: pp. 309–406.
[20] Morris AP, Thomas PD (1996) Neck Injuries in the UK Co-operative Crash Injury Study. *Proceedings of the Stapp Car Crash Conference*, 1996, Warrendale, PA: Society of Automotive Engineers , pp. 317–29.
[21] Temming J, Zobel R (1998) Frequency and Risk of Cervical Spine Distortion Injuries in Passenger Car Accidents: Significance of Human Factors Data. *Proceedings of the IRCOBI Conference*, Gothenburg, Sweden.
[22] Krafft M, Kullgren A, Lie A, Tingvall C (2003) The Risk of Whiplash Injury in the Rear Seat Compared to the Front Seat in Rear Impacts. *Traffic Injury Prevention, 2003*, **4**: pp. 136–40.
[23] Jakobsson L, Norin H, Svensson MY (2004) Parameters Influencing AIS 1 Neck Injury Outcome in Frontal Impacts. *Traffic Injury Prevention*, 2004, **5**: pp. 156–63.

[24] Carstensen TB *et al.* (2012) Are there Gender Differences in Coping with Neck Pain Following Acute Whiplash Trauma? A 12-Month Follow-up Study. *European Journal of Pain*, 2012, **16**: pp. 49–60.
[25] Bose D, Segui-Gomez M, Crandall JR (2011) Vulnerability of Female Drivers Involved in Motor Vehicle Crashes: An Analysis of US Population at Risk. *The American Journal of Public Health*, 2011, **101**(12): pp. 2368–73.
[26] Gayzik FS *et al.* (2009) A Multi-Modality Image Data Collection Protocol for Full Body Finite Element Model Development. *SAE Technical Paper 2009-01-2261*. SAE International, 2009, Warrendale, PA, USA.
[27] Gayzik FS *et al.* (2011) Development of a Full Body CAD Dataset for Computational Modeling: A Multi-Modality Approach. *Annals of Biomedical Engineering*, 2011, **39**(10): pp. 2568–83.
[28] Gordon CT *et al.* (1989) *1988 Anthropometric survey of U.S. army personnel: Methods and summary statistics*. United States Army Natick Research Development and Engineering Center, Natick, MA.
[29] Panjabi MM, Brand RA, White A. (1976) Mechanical Properties of the Human Thoracic Spine As Shown by Three-Dimensional Load-Displacement Curves. *The Journal of Joint and Bone Surgery*, 1976, **58-A**(5): pp. 642–52.
[30] Panjabi MM, Oxland TR, Yamamoto I, Crisco JJ (1994) Mechanical Behavior of the Human Lumbar and Lumbosacral Spine as Shown by Three-Dimensional Load-Displacement Curves. *The Journal of Joint and Bone Surgery*, 1994, **76-A**: pp. 413–24.
[31] Asano S, Kaneda K, Umehara S, Tadano S (1992) The Mechanical Properties of the Human L4-5 Functional Spinal Unit during Cyclic Loading. *Spine*, 1992, **17**(11): pp. 1343–52.
[32] Lu WW, Luk KDK, Holmes AD, Cheung KMC, Leong JCY (2005) Pure Shear Properties of Lumbar Spinal Joints and the Effect of Tissue Sectioning on Load Sharing. *Spine*, 2005, **30**(8): pp. E204–9.
[33] Valentin J (2002) Basic Anatomical and Physiological Data for the Use in Radiological Protection: Reference Values. *Annals of the ICRP*, 2002, 1–227.
[34] Duprey S, Subit D, Guillemot, Kent RW (2010) Biomechanical Properties of the Costovertebral Joint. *Medical Engineering and Physics*, 2010, **32**: pp. 222–227.
[35] Manschott JFM, Brakkee AJM (1986) The Measurement and Modelling of the Mechanical Properties of Human Skin in Vivo – II. The Model. *Journal of Biomechanics*, 1986, **19**(7): pp. 517–21.
[36] Engelbrektsson K (2011) *Evaluation of Material Models in LS-DYNA for Impact Simulation of White Adipose Tissue*. MSc. Thesis, Chalmers University of Technology, Gothenburg, Sweden. Available at: http://publications.lib.chalmers.se/records/fulltext/147789.pdf
[37] Kindig M, Li Z, Kent R, Subit D (2015) Effect of Intercostal Muscle and Costovertebral Joint Material Properties on Human Ribcage Stiffness and Kinematics. *Computer Methods in Biomechanics and Biomedical Engineering*, 2015, **18**(5): pp. 556–70.
[38] Forman J, Del Pozo de Dios, Kent RW (2010) A Pseudo-Elastic Effective Material Property Representation of the Costal Cartilage for Use in Finite Element Models of the Whole Human. *Traffic Injury Prevention*, 2010, **11**(6): pp. 613–22.
[39] Wood GW, Panzer MB, Bass CR, Myers BS (2010) Viscoelastic Properties of Hybrid III Head Skin. *SAE International Journal of Materials Manufacturing*, 2010, **3**(1): pp. 186–93.
[40] Roach KE, Miles TP (1991) Normal Hip and Knee Active Range of Motion: The Relationship to Age. *Physical Therapy*, 1991, **71**: 656–665.
[41] Ludewig PM *et al.* (2009) Motion of the Shoulder Complex During Multiplanar Elevation. *The Journal of Bone and Joint Surgery*, 2009, **91**: pp. 378–89.
[42] Standring S. (ed.) (2008) *Gray's Anatomy – The Anatomical Basis of Clinical Practice. Elsevier Churchill Livingstone*, London, UK.
[43] Engin AE, Chen SM (1987) Kinematic and Passive Resistive Properties of Human Elbow Complex. *Journal of Biomechanical Engineering*, 1987, **109**: pp. 318–23.
[44] Östh J, Brolin K, Svensson MY, Linder A (2016). A Female Ligamentous Cervical Spine Finite Element Model Validated for Physiological Loading. *Journal of Biomechanical Engineering* **138**(6).
[45] Östh J *et al.* (2017) A Female Head-Neck Model for Rear Impact Simulations. *Journal of Biomechanics*, 2017, **51**: pp. 49–56.
[46] Panjabi MM *et al.* (1986) Three-Dimensional Load-Displacement Curves due to Forces on the Cervical Spine. *Journal of Orthopaedic Research*, 1986, **4**: pp. 152–61.
[47] Panjabi MM *et al.* (2001) Mechanical Properties of the Human Cervical Spine as Shown By Three-Dimensional Load-Displacement Curves. *Spine* 2001, **26**: pp. 2692–700.

[48] Nightingale RW *et al.* (2002) Comparative Strengths and Structural Properties of the Upper and Lower Cervical Spine in Flexion and Extension. *Journal of Biomechanics*, 2002, **35**: pp. 725–32.
[49] Shaw G *et al.* (2009) Impact Response of Restrained PMHS in Frontal Sled Tests: Skeletal Deformation Patterns Under Seat Belt Loading. *Stapp Car Crash Journal*, 2009, **53**: pp. 1–48.
[50] Ash JH *et al.* (2012) Whole-Body Kinematics: Response Corridors for Restrained PMHS in Frontal Impacts. *Proceedings of the IRCOBI Conference*, 2012, Dublin, Ireland.
[51] Lessley DJ *et al.* (2014) Occupant Kinematics in Laboratory Rollover Tests: PMHS Response. *Stapp Car Crash Journal*, 2014, **58**: pp. 251–316.
[52] Yoganandan N *et al.* (2000) Biomechanics of Human Occupants in Simulated Rear Crashes: Documentation of Neck Injuries and Comparison of Injury Criteria. *Proceedings of the Stapp Car Crash Conference,* 2000*,* Warrendale, PA: Society of Automotive Engineers.
[53] TU Delft, "DINED Anthropometric Database" Internet: [http://dined.io.tudelft.nl/en/], Accessed 20 December 2016.
[54] Zhang Q *et al. (2013)* Whole-Body Kinematics: Response Comparison of the Hybrid III and Hybrid III Pedestrian ATD in DRoTS Rollover Tests. *Proceedings of the IRCOBI Conference*, 2013, Gothenburg, Sweden.
[55] Deng B, Begeman PC, Yang KH, Tashman S, King AI (2000) Kinematics of Human Cadaver Cervical Spine during Low-Speed Rear-End Impacts. *Proceedings of the 44th Stapp Car Crash Conference*, 2000, Atlanta, Georgia.
[56] Kang Y-S *et al.* (2012). Biomechanical Responses of PMHS in Moderate-Speed Rear Impacts and Development of Response Targets for Evaluating the Internal and External Biofidelity of ATDs. *Stapp Car Crash Journal*, 2012, **56**: pp. 105–70.
[57] Sundarajan S *et al.* (2004). Effect of Head-Neck Position on Cervical Facet Stretch of Post Mortem Human Subjects during Low Speed Rear End Impacts. *Stapp Car Crash Journal*, 2004, **48**: pp. 1–42.
[58] White NA *et al.* (2009) Investigation of Upper Body and Cervical Spine Kinematics of Post Mortem Human Subjects (PMHS) during Low-Speed, Rear-End Impacts. *SAE Technical Paper 2009-01-0387*. SAE International, 2009, Warrendale, PA, USA.
[59] Mertz H (1984) A Procedure for Normalizing Impact Response Data. *SAE Technical Paper 840884*. SAE International, 1984, Warrendale, PA, USA.
[60] Meijer R, Wigershof R, Wismans J, Been B (2009) Scaling Head-Neck Response Data and Derivation of 5th Percentile Female Side-Impact Dummy Head-Neck Response Requirements in NBDL Test Conditions. *International Journal of Crashworthiness*, 2009, **14**: pp. 233–43.
[61] Gehre C, Gades H, Wernicke P (2009) Objective Rating of Signals using Test and Simulation Responses. *Proceedings of the 24th ESV conference*, 2009, Stuttgart, Germany.
[62] Sato F *et al.* (2017). Effects of Whole Spine Alignment Patterns on Neck Responses in Rear End Impact. *Traffic Injury Prevention*, 2017, **18**(2): pp. 199–206.
[63] Mordaka J (2004) *Finite Element Analysis of Whiplash Injury for Women*, Ph.D. Thesis, Nottingham Trent University, Nottingham, UK.
[64] Stemper BD, Pintar FA, Rao RD (2011) The Influence of Morphology on Cervical Injury Characteristics. *Spine*, 2011, **36**(25S): pp. S180–86.
[65] Shi X, Chao L, Reed MP, Rupp JD, Hu J (2015) Effects of Obesity on Occupant Responses in Frontal Crashes: A Simulation Analysis using Human Body Models. *Computer Methods in Biomechanics and Biomedical Engineering*, 2015, **18**(12): pp. 1280–92.
[66] Mattucci SFE, Moulton JA, Chandrashekar N, Cronin DS (2012) Strain Rate Dependent Properties of Younger Human Cervical Spine Ligaments. *Journal of the Behavior of Biomedical Materials*, 2012, **41**: pp. 216–26
[67] Stemper BD, Board D, Yoganandan N, Wolfla CE (2010) Biomechanical Properties of Human Thoracic Spine Disc Segments. *Journal of Craniovertebral Junction and Spine*, 2010, **1**(4): pp. 18–22.
[68] Broos J, Meijer R (2016). Simulation Method for Whiplash Injury Prediction Using an Active Human Model. *Proceedings of the IRCOBI Conference, 2016*, Malaga, Spain.
[69] Feller L, Kleinbach C, Fehr J, Schmitt S. Incorporating Muscle Activation Dynamics into the Global Human Body Model. *Proceedings of the IRCOBI Conference, 2016*, Malaga, Spain.
[70] Östh J, Brolin K, Carlsson S, Wismans J, Davidsson J (2012) The Occupant Response to Autonomous Braking: A Modeling Approach That Accounts for Active Musculature. *Traffic Injury Prevention* **13**(3): pp. 265–77.
[71] Camacho DL *et al.* (1997) Experimental Flexibility Measurements for the Development of a Computational Head-Neck Model Validated for Near-Vertex Head Impact. *Proceedings of the 41st Stapp Car Crash Conference*. Warrendale, PA: Society of Automotive Engineers, 1997, pp. 473–86.

## VIII. Appendix A: Additional Kinematic Response and Seat Belt Forces in the Whole Body Simulations

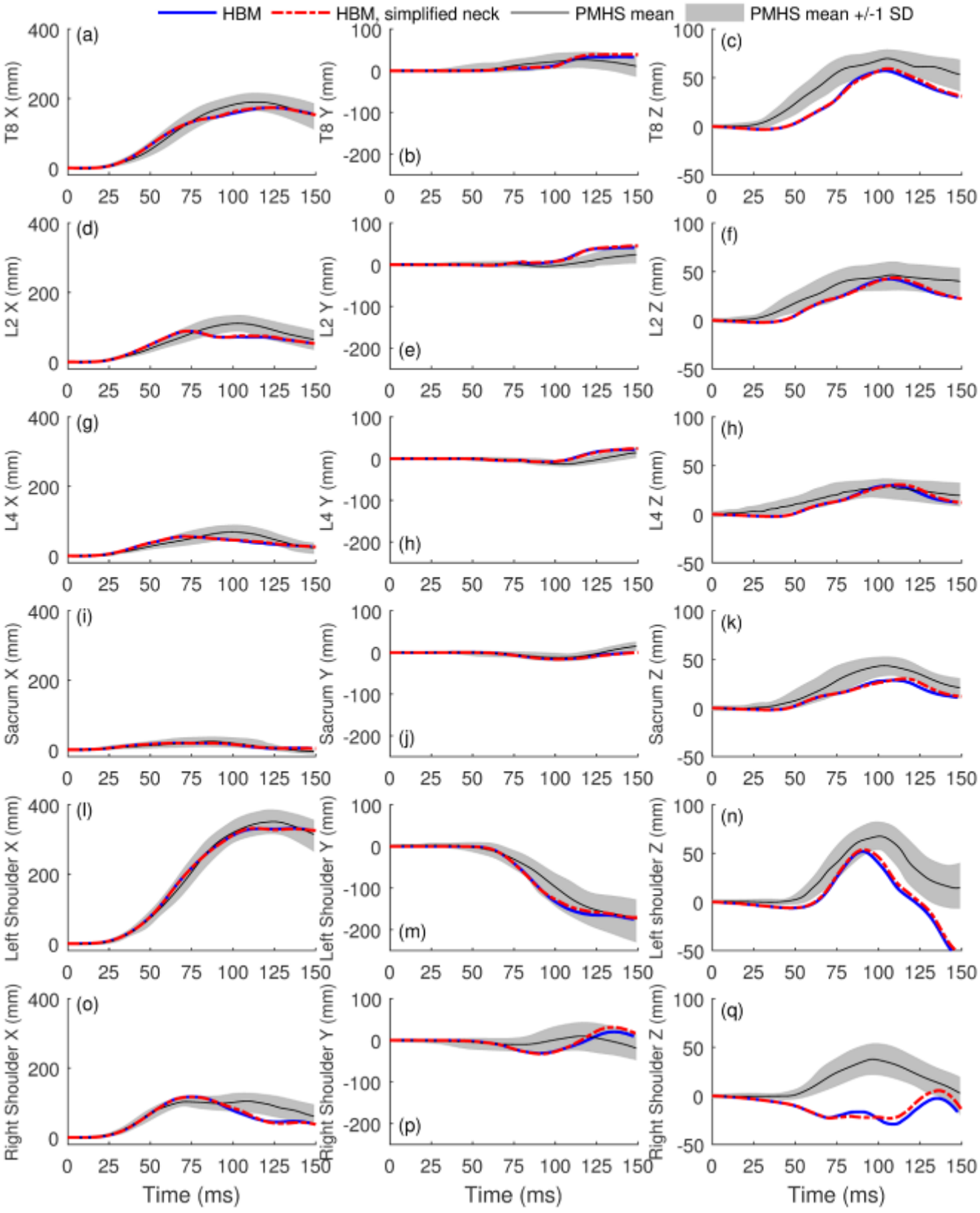


Fig. A1. T8, L2, L4, sacrum and shoulder kinematics of the HBM in the frontal impact simulations, compared with that of scaled PMHS data [49, 50]. SD = Standard Deviation.

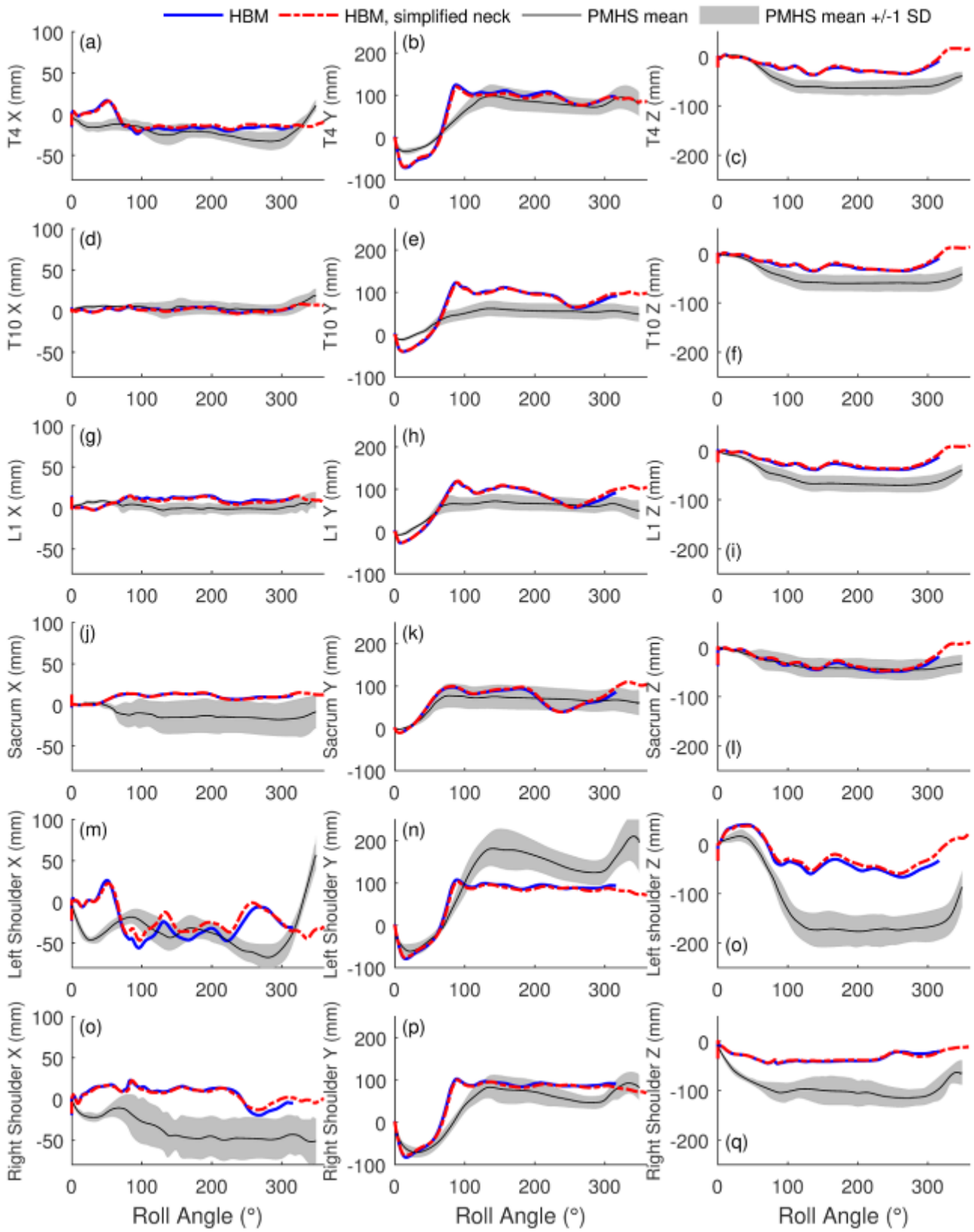


Fig. A2. T4, T10, L1, sacrum and shoulder kinematics of the HBM relative to the buck roll-angle in the roll-over simulations, compared with that of scaled PMHS data [51]. SD = Standard Deviation.

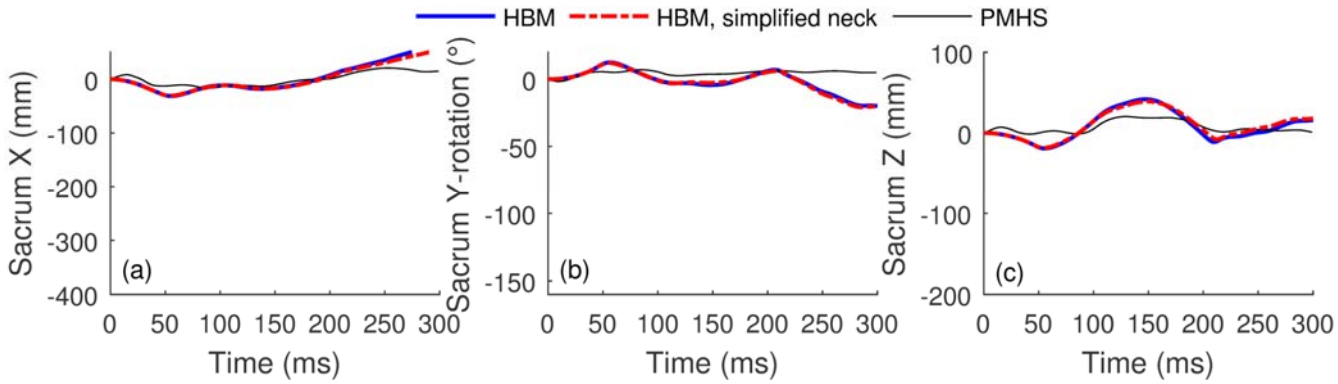


Fig. A3. Sacrum kinematics in the rear-impact simulations, compared with that of one female PMHS [52].

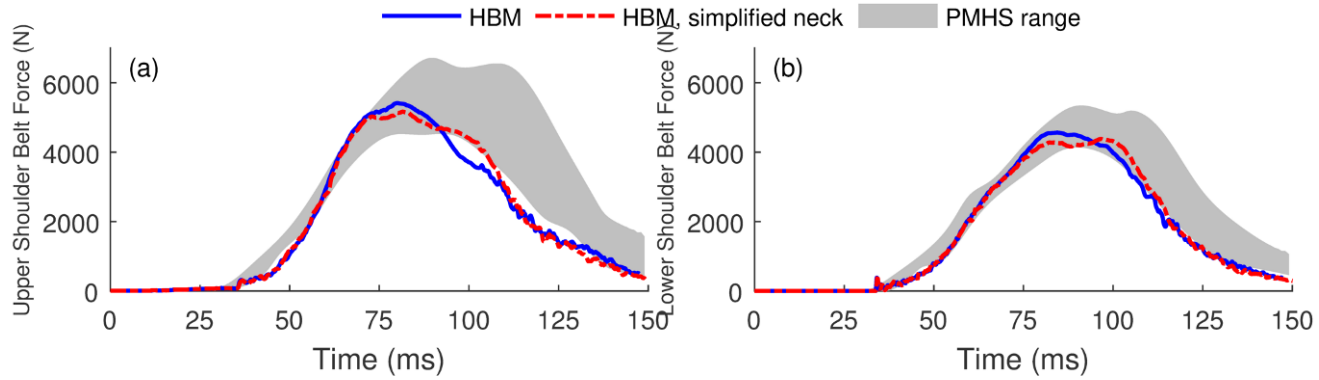


Fig. A4. Shoulder belt forces measured above (upper) the shoulder (a), and below the chest (lower) (b) in the HBM in the frontal impact simulations, compared with that of the of scaled range (maximum and minimum envelope) of the PMHS data [49, 50].

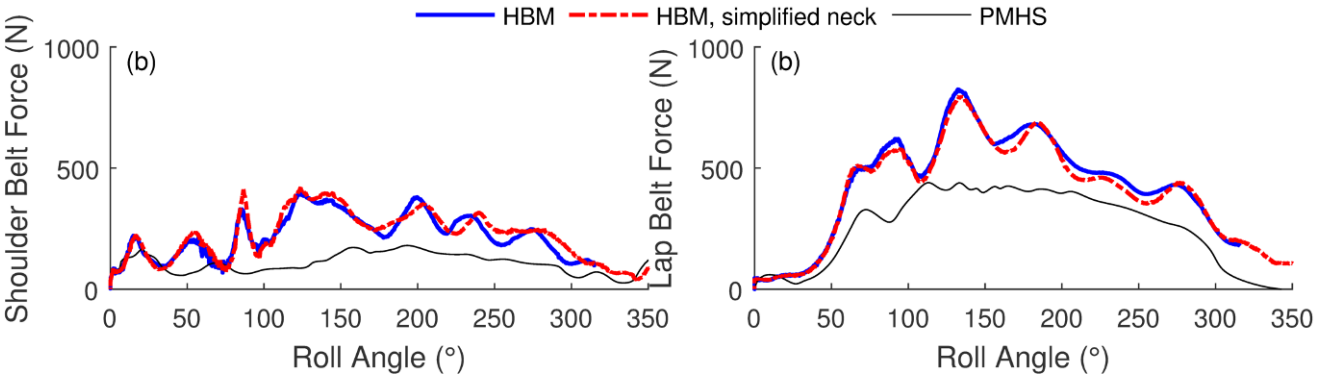


Fig. A5. Shoulder-belt (a) and lap-belt (b) forces of the HBM relative to the buck roll-angle in the roll-over simulations, compared with that of scaled PMHS mean [51].

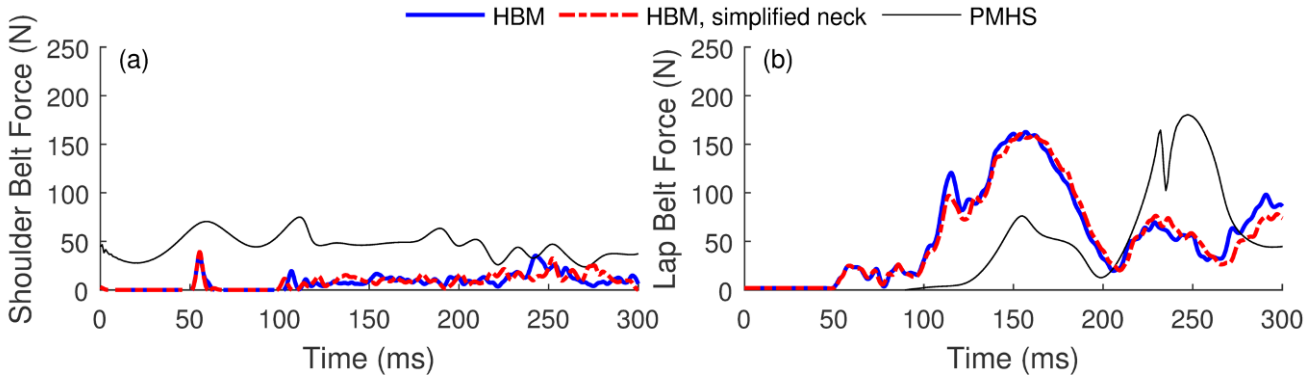


Fig. A6. Shoulder-belt (a) and lap-belt (b) forces in the rear-impact simulations, compared with that of one female PMHS [52].

## IX. Appendix B: Cervical Spine Posture Sensitivity in Rear-impact

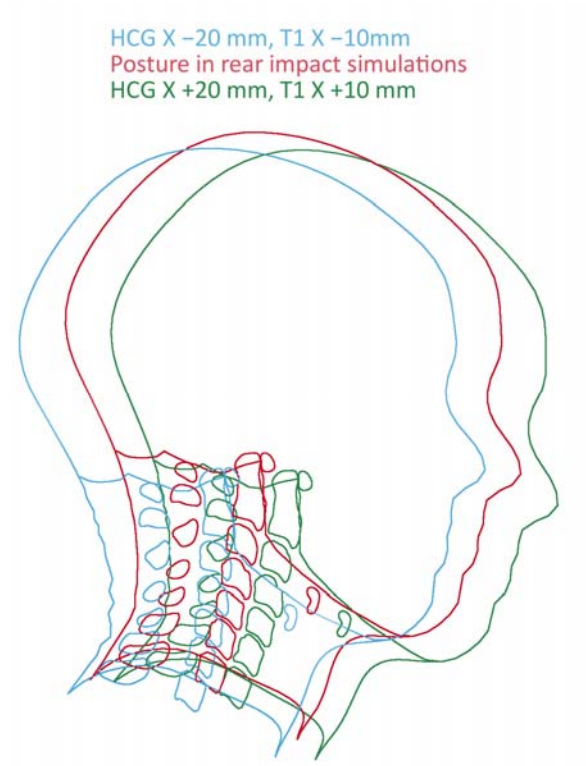


Fig. B1. Cervical spine postures used in the sensitivity study. HCG = Head Centre of Gravity.

With the more forward head position, the HBM captured some of the trend with an initial upward head movement as the spine straightens out, together with some positive Z-rotation (Fig. B2). This led to a better correlation with the PMHS results (Table B1), while the more rearward head position led to an almost equal grand total correlation as in the reference posture described in Section II.

Table B1

Objective rating results of whole body simulations.

The shaded columns represent the primary kinematics variable in the rear-impact load case. Total is the weighted [61] sum of each column, while the grand total for each load case is the weighted sum of each total for the load case.

| **HBM with detailed neck** | | | | | | | | | |
|---|---|---|---|---|---|---|---|---|---|
| | **Rearward posture** | | | **Rear-impact** | | | **Forward posture** | | |
| | X | Y-rotation | Z | X | Y-rotation | Z | X | Y-rotation | Z |
| Head | 0.66 | 0.74 | 0,32 | 0.7 | 0.76 | 0.29 | 0.75 | 0.82 | 0.35 |
| T1 | 0.69 | 0.71 | 0.42 | 0.78 | 0.59 | 0.3 | 0.91 | 0.76 | 0.44 |
| Sacrum | 0.43 | 0.25 | 0.26 | 0.41 | 0.25 | 0.36 | 0.44 | 0.26 | 0.3 |
| Total | **0.59** | **0.57** | 0.33 | **0.63** | **0.53** | 0.32 | **0.70** | **0.61** | 0.36 |
| Grand total | 0.50 | | | 0.49 | | | 0.56 | | |

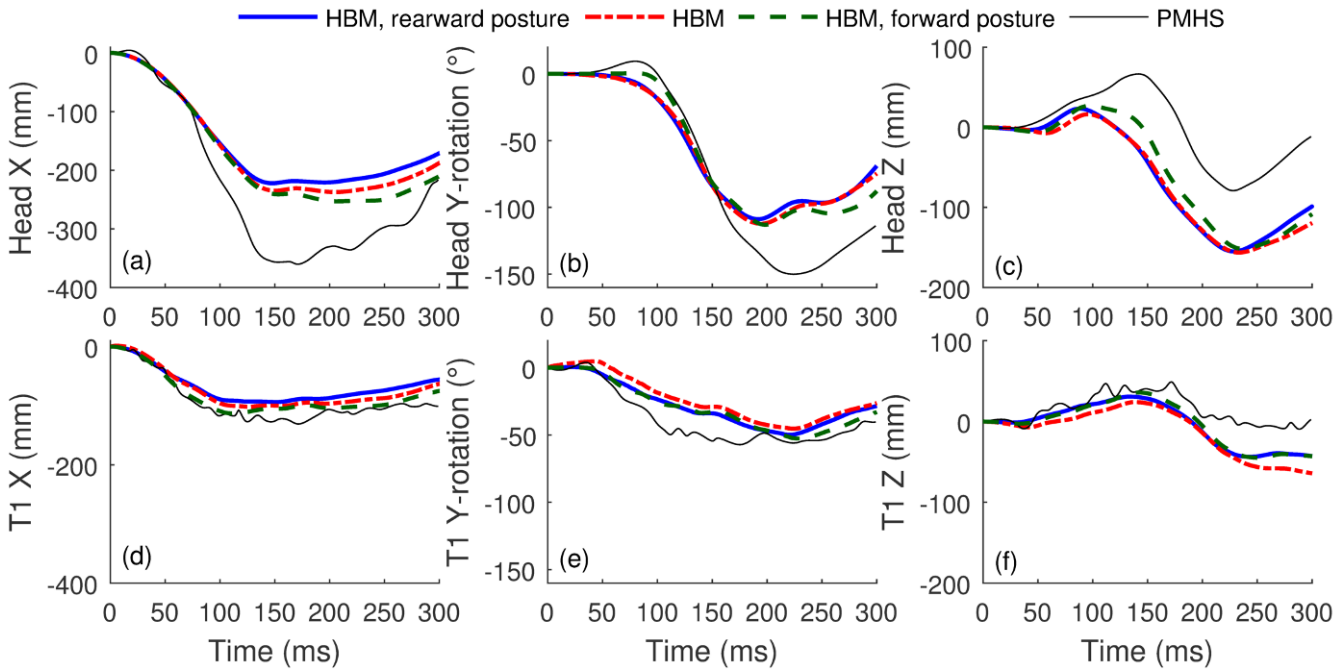


Fig. B2. Head and T1 kinematics in the rear-impact cervical spine posture parameter study simulations, compared with that of one female PMHS [52].

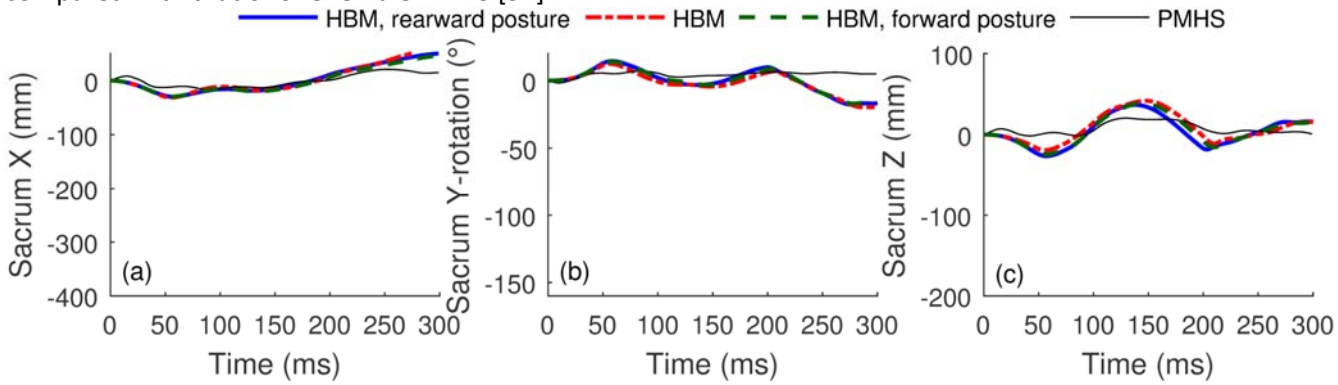


Fig. B3. Sacrum kinematics in the rear-impact cervical spine posture parameter study simulations, compared with that of one female PMHS [52].

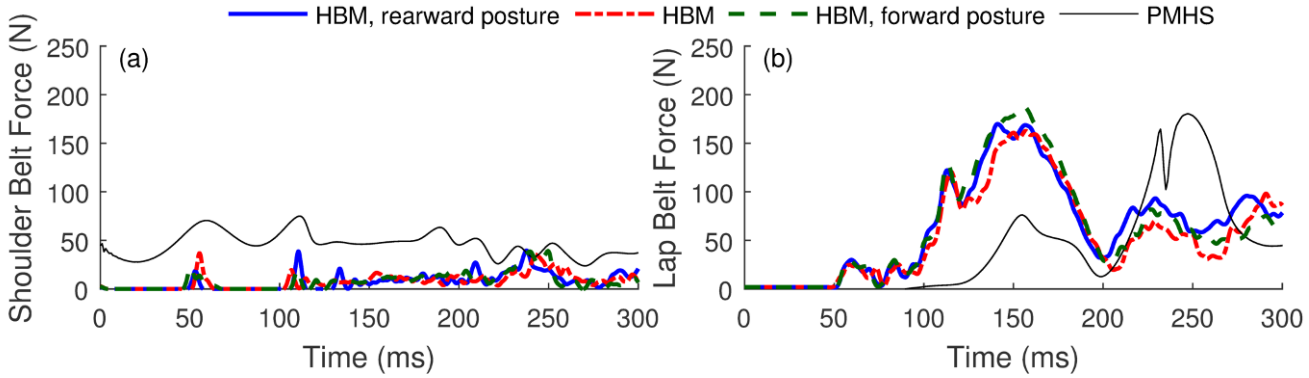


Fig. B4. Shoulder-belt (a) and lap-belt (b) forces in the rear-impact cervical spine posture parameter study simulations, compared with that of one female PMHS [52].

## X. APPENDIX C: MANUAL PAGES FOR THE VIVA OPENHBM FINITE ELEMENT 50TH PERCENTILE FEMALE OCCUPANT MODEL

This appendix contains user manual information for the VIVA OpenHBM Finite Element 50$^{th}$ Percentile Female Occupant Model.

### *Running the HBM*

The HBM has been developed using the parallel version of LS-DYNA (LSTC, Livermore, CA) MPP-DYNA version R8.1.0 with Intel MPI v5.0 software, on Intel Xeon E5-2650V3 cluster machines running CentOS release 6.8. Both single and double precision simulations have been run successfully. Shared Memory Parallel (SMP) binaries of LS-DYNA have not been tested, but it has been reported that the model is not numerically stable in SMP simulations. The keyword files for the model are structured according to Table C1.

TABLE C1. KEYWORD FILE STRUCTURE FOR THE HBM.
YYYYMMDD = YEAR (YYYY), MONTH (MM), AND DAY (DD) THE MODEL FILE WAS UPDATED.

| File name | Content |
|---|---|
| run_VIVA_OpenHBM_F50_YYYMMDD.key | Main file. Open this file in a pre-processor to open the whole model. |
| VIVA_OpenHBM_F50_Control_YYYMMDD.key | LS-DYNA control cards. |
| VIVA_OpenHBM_F50_Geom_YYYMMDD.key | All geometry related entities, such as node and element data, but also contact segments and node sets. |
| VIVA_OpenHBM_F50_HN_Contacts_YYYMMDD.key | Contacts for the head and neck. |
| VIVA_OpenHBM_F50_HN_Part_Data_YYYMMDD.key | Part, section, and material data for the head and neck. |
| VIVA_OpenHBM_F50_LOWEX_Part_Data_YYYMMDD.key | Part, section and material data for the lower extremities. |
| VIVA_OpenHBM_F50_T_Contacts_YYYMMDD.key | Contacts for the torso. |
| VIVA_OpenHBM_F50_T_Part_Data_YYYMMDD.key | Part, section and material data for the torso. |
| VIVA_OpenHBM_F50_UPEX_Part_Data_YYYMMDD.key | Part, section and material data for the upper extremities. |

### *Units and Coordinates*

All model files are defined in the unit system mm-ms-kg-kN, which means that the default stress unit is GPa (kN/mm$^2$). The model global coordinate system has its origin in the H-point (in the midplane of the human body, at the location of the hip articulation), with positive X forward, positive Y to the left, and positive Z upwards (see Fig. 1).

***Model Structure***

The HBM is structured in to nine body sections, Fig. C1. In each section, the LS-DYNA part identity numbers (PIDs) occupy the range X 000 000–X 099 999, the shell element numbers the range X 100 000–X 499 999, the solid element numbers the range X 500 000–X 799 999, and the beam and discrete elements the range X 800 000–X 999 999. Here X is the section number according to Fig. C1. In addition, nodal identification numbers (NIDs) range from X 000 000 to X 999 999 for each section X. For example, the cortical bone of the skull has the PID 1002001, contains the shell element 1100729, and this shell is defined by the nodes 1004034, 1004028, 1004026 and 1004026.

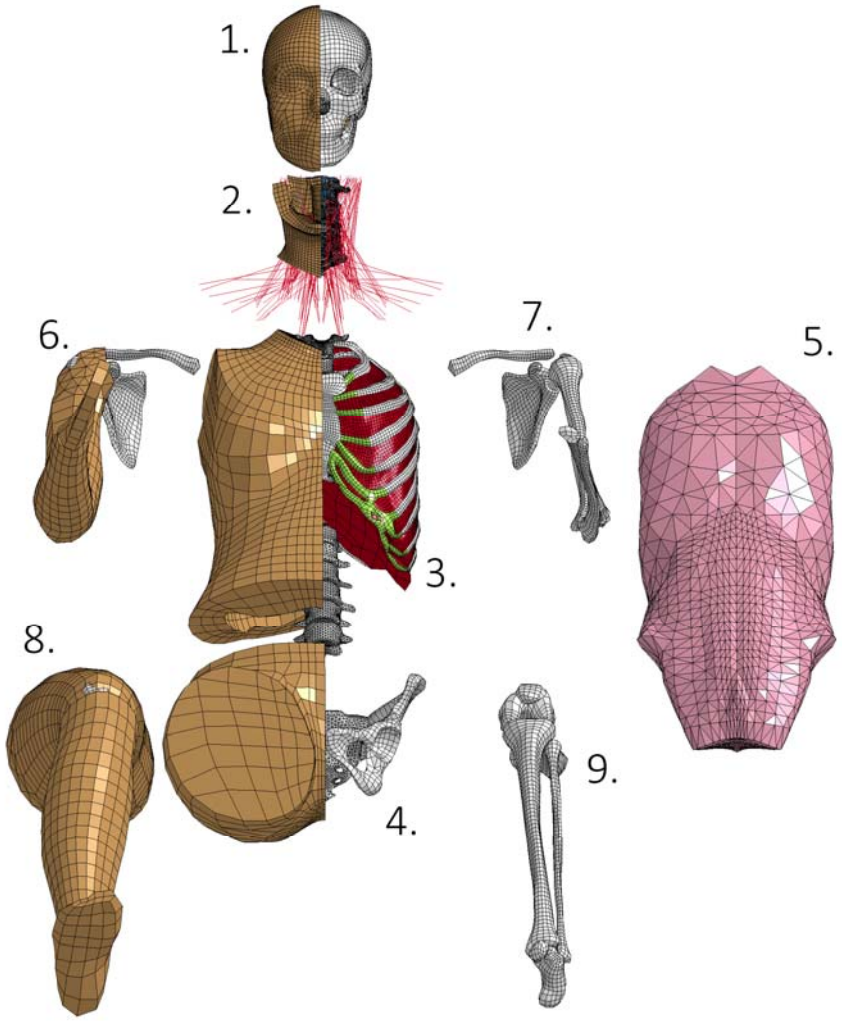


Fig. C1. Sectioning and numbering of the HBM.

TABLE C2. BODY SECTIONS OF THE HBM.

| Number | Body Section | Start Part ID | Part Name Prefix |
|---|---|---|---|
| 1. | Head | 1 000 000 | H_ |
| 2. | Neck | 2 000 000 | N_ |
| 3. | Torso | 3 000 000 | T_ |
| 4. | Pelvis | 4 000 000 | P_ |
| 5. | Thoracic cavities/Internal organs | 5 000 000 | IO_ |
| 6 | Right Upper Extremity | 6 000 000 | RUX_ |
| 7. | Left Upper Extremity | 7 000 000 | LUX_ |
| 8. | Right Lower Extremity | 8 000 000 | RLX_ |
| 9. | Left Lower Extremity | 9 000 000 | LLX_ |

***Naming and Numbering Conventions***

In most cases, each individual part has its own section and material card, with the same ID number as the PID. PIDs are assigned in the intervals defined in Table C1, and depending on the type of tissue in the human body the part represents a sub-interval and second pre-fix according to TABLE C3 is used.

TABLE C3. SUB-INTERVAL AND SECOND PRE-FIX FOR PARTS REPRESENTING DIFFERENT TISSUE TYPES ACCORDING TO THE USED NAMING CONVENTION.

| Tissue type | Sub-interval | Second Pre-fix |
|---|---|---|
| Trabecular bone | X 001 000 | _TB_ |
| Cortical bone | X 002 000 | _CB_ |
| Cartilage | X 003 000 | _C_ |
| Ligament | X 004 000 | _L_ |
| Flesh | X 005 000 | _F_ |
| Adipose Tissue | X 006 000 | _A_ |
| Tendon | X 007 000 | _T_ |
| Muscle | X 008 000 | _M_ |
| Skin | X 009 000 | _S_ |
| Soft Tissue (general) | X 010 000 | _ST_ |
| Null | X 011 000 | _N_ |
| Joint (Beam) | X 500 000 | _J_ |

The part, material, and section card for the inferior facet joint cartilage of the C3 vertebra is shown in **Fel! Hittar inte referenskälla.** as an example of the naming and numbering convention used.

```
*PART
$#                                                                         title
N_C_C3-Inf_Facet_Art_Cart
$#     pid     secid       mid     eosid      hgid      grav    adpopt      tmid
   2003013   2003013   2003013         0   2000000         0         0         0
*SECTION_SOLID
$#   secid    elform       aet
   2003013         1         0
*MAT_ELASTIC
$#     mid        ro         e        pr        da        db  not used
   2003013 1.0000E-6 0.0100000  0.400000     0.000     0.000         0
```

Fig. C2. Sample part, material, and section card for the C3 inferior facet joint cartilage.

***Modelling Requirements***

The target critical time step for the HBM is selected to 0.3 µs. This critical time step corresponds to a critical element length of 1 mm for a shell element made of cortical bone (E=17.1 GPa, v=0.3, ρ=2000 kg/m$^3$) with a time scale factor of 0.9 (default in LS-DYNA). In addition, the mesh has been developed aiming for the mesh quality criteria in TABLE C4. All contacts have been verified to be free from initial penetrations, by setting the parameter IGNORE=2 on the *CONTROL_CONTACT card so that LS-DYNA reports if any initial penetrations are found by the contact algorithms.

TABLE C4. MESH QUALITY CRITERIA.

| **Shell Element Criteria** | **Requirement** |
|---|---|
| Aspect ratio | <3.0 |
| Skewness | <30 |
| Warpage | <7° |
| Taper | >0.5 |
| Quad Angle | 45°<$\alpha$<135° |
| Tria Angle | 30°<$\alpha$<120° |
| **Solid Element Criteria** | **Requirement** |
| Aspect ratio | <3.0 |
| Jacobian | >0.4 |
| Skewness | >0.5 |
| Warpage | <10° |